Article

Gas-Phase Room-Temperature Detection of the *tert*-Butyl Hydroperoxide Dimer

Published as part of The Journal of Physical Chemistry virtual special issue "Marsha I. Lester Festschrift".

Casper Vindahl Jensen and Henrik G. Kjaergaard*

Read Online

ACCESS | Metrics & More | Article Recommendations | Supporting Information

ABSTRACT: We have detected the *tert*-butyl hydroperoxide dimer, (t-BuOOH)$_2$, in the gas phase at room temperature using conventional FTIR techniques. The dimer is identified by an asymmetric absorbance band assigned to the fundamental hydrogen-bound OH$_b$-stretch. The weighted band maximum of the dimer OH$_b$-stretch is located at ~3452 cm^{-1}, red-shifted by ~145 cm^{-1} from the monomer OH-stretching band. The gas-phase dimer assignment is supported by Ar matrix isolation FTIR experiments at 12 K and experiments with a partially deuterated sample. Computationally, we find the lowest energy structure of (t-BuOOH)$_2$ to be a doubly hydrogen bound six-membered ring with non-optimal hydrogen bond angles. We estimate the gas-phase constant of dimer formation, K, to be 0.4 (standard pressure of 1 bar) using the experimental integrated absorbance and a theoretically determined oscillator strength of the OH$_b$-stretching band.
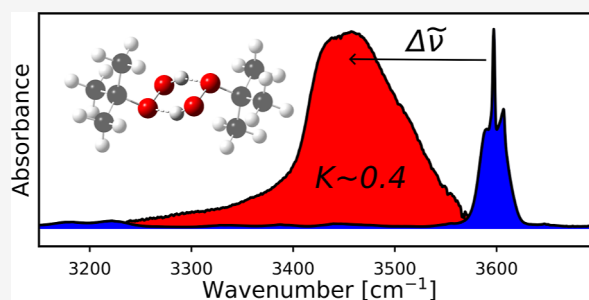
INTRODUCTION

Hydrogen bonds are of general interest and the formation of hydrogen bound complexes are important in a myriad of chemical systems. These range from particle formation and aerosol growth in the atmosphere to biological processes where inter- and intramolecular hydrogen bonds are key to the shape and functionality of proteins.[1-5] In the atmosphere, volatile organic compounds are emitted and subsequently oxidized, leading to a large presence of highly oxygenated organic molecules (HOMs) capable of acting as hydrogen bond donors and/or acceptors. These HOMs include functionalities such as alcohols, hydroperoxides, organic acids, ethers, carbonyls, etc.[6] Hydrogen bonds play a crucial role in the formation of the initial bimolecular complexes that grow to form larger clusters, which ultimately condense into aerosols and particles in the atmosphere.[7,8] Formation of bimolecular complexes with a single hydrogen bond are usually energetically disfavored compared to the monomers at room temperature due to the small binding enthalpies and low entropy of the complexes. This results in relatively small unitless formation constants (standard pressure of 1 bar), typically $K < 1$.[9] In contrast, carboxylic acids form doubly hydrogen bound dimers with geometries that allow for optimal hydrogen bonding angles of ca. 180° in a planar eight-membered ring.[10,11] Carboxylic acids therefore have significantly larger constants of dimer formation of $K > 100$.[12-21]

Previously, it has been shown that the organic hydroperoxide, *tert*-butyl hydroperoxide (*t*-BuOOH) forms stronger hydrogen bonds, compared to the corresponding alcohol *tert*-butanol (*t*-BuOH).[22] In the complexes with di-methyl ether (DME) as acceptor (O-atom), the observed room temperature gas phase OH-stretching redshift increased from ~100 cm^{-1} for the *t*-BuOH·DME complex to ~170 cm^{-1} for the *t*-BuOOH·DME complex, and K was found to be 5.5 times higher for the *t*-BuOOH·DME complex. Bimolecular complexes consisting of two hydroperoxide units have been detected in cold matrix isolation experiments and ab initio calculations have suggested a doubly hydrogen-bound structure.[23-29] These complexes include H$_2$O$_2$ dimer, HO$_2$ dimer, and the H$_2$O$_2$−HO$_2$ complex. The geometry of these doubly bound complexes are suggested to have a ring-type structure similar to that of the organic acids; however, with a non-planar six-membered ring. In CCl$_4$ solution, (t-BuOOH)$_2$ has been detected with the same suggested doubly bound cyclic structure and an equilibrium constant of $K = 1.9$.[30]

Organic hydroperoxides are known to be unstable and even explosive under ambient conditions and therefore warrant concerns when handled.[31] *t*-BuOOH is a somewhat stable organic hydroperoxide, which makes it well-suited for experimental studies. It has been used as a model compound
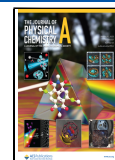
for the organic hydroperoxide functionality in studies of properties such as the OH-stretching overtone spectroscopy, OH-stretch coupling to the COOH torsion and photo-dissociation of the OO-bond, with various gas phase infrared (IR) and ultra violet-visible spectroscopic techniques as well as with theoretical simulations.[32−38]

In this study, we detect the t-BuOOH dimer $(t$-BuOOH$)_2$ in the gas phase at room temperature. To the best of our knowledge, this is the first gas phase detection of an organic hydroperoxide dimer at room temperature. The low vapor pressure of t-BuOOH ($\sim$5 Torr) present an experimental challenge, as the formation of dimer scales with its formation constant and the monomer pressure squared. The absorbance band associated with the hydrogen bound OH$_b$-stretching fundamental transition in the dimer is assigned and quantified. We estimate the constant of dimer formation, K, by an approach that combines spectroscopic measurements and a calculated oscillator strength of the associated OH$_b$-stretching band.[9] We compare the results to that previously reported for $(t$-BuOOH$)_2$ in CCl$_4$ solution, the singly bound t-BuOOH· DME complex and acetic acid dimer and complex to elucidate the effects of the number of hydrogen bonds as well as the functional groups involved in the bonding.[9,12−22,39] Additionally, the weak interactions between the two t-BuOOH units in the dimer are illustrated by a non-covalent interaction (NCI) analysis.[40−43]

EXPERIMENTAL SECTION

The compounds t-BuOOH in water (70 wt %), t-BuOOH in decane (5.0−6.0 M), t-BuOH (anhydrous, ≥99.5%), DCM (anhydrous, ≥99.8%), MgSO$_4$ (anhydrous, ≥99.5%), and molecular sieves (3 Å) were purchased from Sigma-Aldrich. Deuterium oxide was purchased from Eurisotop. The water solvated t-BuOOH sample was extracted into DCM by a liquid−liquid phase extraction. The DCM phase was then dried by adding MgSO$_4$. To make the partially deuterated sample, the water solvated t-BuOOH sample was mixed with deuterium oxide in volume ratio 1:2 by stirring for 2 h and the DCM phase extraction was performed afterward. All samples were kept in sample holders sealed by PRODURAN Teflon stoppers. All samples, except for t-BuOH, which was semi-solid at the working temperatures, were ensured dry by adding activated 3 Å molecular sieves to the sample holders. The samples were connected via Swagelok UltraTorr fittings to a J. Young vacuum line with a background pressure of 10^{-4} Torr and were degassed repeatedly by freeze-pump-thaw-cycles until no bubbles were observed upon thawing.

The sample gas was introduced directly via a flexible metal tube into a 1 m optical pathlength cell (Tornado Series T5, Specac White-cell). The cell was fitted with CaF$_2$ windows and Au-coated internal and Al external mirrors and was placed in a Fourier transform IR (FTIR) (Bruker Vertex 80) spectrometer. The vacuum system and cell was flushed with D$_2$O before conducting the deuterium experiments to limit the rapid H/D exchange with trace amounts of H$_2$O. The cell compartment was continuously purged with N$_2$ during measurements to limit absorption from ambient H$_2$O and CO$_2$. The sample holders were covered with duct tape and the glass vacuum line and sample cells were covered in black plastic at all times to reduce photo-degradation of t-BuOOH. The pressure was measured in 10 s intervals by a diaphragm pressure gauge (Agilent, CDG500—10 Torr) attached directly to the cell. From this measurement, the monomer pressure was obtained

by subtracting the estimated partial pressures of the solvent and impurities (vide infra). The temperature around the sample cells was kept at 298.2 ± 0.2 K during the recording of the spectra.

All spectra were recorded with a KBr beam splitter, a liquid nitrogen cooled HgCdTe (LN-MCT) detector with scanning velocity of 80 kHz and were averaged over 2000 scans with a 1 cm^{-1} resolution. We used a near IR (NIR) light source with a 3 mm aperture. This light source/beamsplitter/detector combination gave the highest S/N ratio for the OH$_b$-stretch region and the higher wavenumber region of the DCM reference band facilitating its subtraction (vide infra).

A low pressure reference spectrum of the t-BuOOH monomer was recorded with a longer optical pathlength cell (16 PA, IR Analysis, Inc. White-cell). The cell had a measured optical pathlength of 15 m and was fitted with KBr windows and Au-coated internal and Al external mirrors. The low sample pressure ($\sim$0.3 Torr) ensured minimal dimer formation in the monomer reference spectrum. The reference spectrum was corrected for DCM and t-BuOH impurities.

At equilibrium, the unitless constant of dimer formation can be expressed by

$$K = \frac{p_{dim} \cdot p^{\ominus}}{p_{mon}^{2}} \qquad (1)$$

where K is the constant of dimer formation, p_{dim} is the dimer pressure, p_{mon} is the monomer pressure, and $p^{\ominus}$ is the standard pressure of 1 bar (750 Torr). To estimate the dimer pressure in the gas mixture we use an experimental and theoretical hybrid technique, which has been described previously.[9,44] We integrate the absorbance of the observed band associated with the OH$_b$-stretch and relate this to a calculated oscillator strength of the transition, f_{calc}, to determine the dimer pressure

$$p_{dim} = 2.6935 \cdot 10^{-9} \frac{\text{Torr m cm}}{\text{K}} \frac{T}{f_{calc} \cdot l} \cdot \int A(\tilde{\nu}) d\tilde{\nu} \qquad (2)$$

where l is the pathlength in units of m, T is the temperature, and $A(\tilde{\nu})$ is the wavenumber-dependent base 10 absorbance.

The dimer pressure is usually hard to obtain directly by experiments as it is insignificant compared to the total pressure of the gas mixture.[9] The hybrid method described has proven efficient at quantifying very small dimer pressures provided a unique absorption band can be detected. The technique takes advantage of the redshift and intensity enhancement of the OH$_b$-stretching band, which typically occurs upon hydrogen bonding.[9−11,45,46]

Matrix isolation experiments were performed to identify complex formation and aid the assignment of the weak $(t$-BuOOH$)_2$ gas phase signal. The t-BuOOH sample was diluted 1:1790 in Ar and deposited on a CsI window at 12 K. A total of 11.7 mmol was deposited at a rate of 0.112 mmol/min. Spectra were recorded at 0.5 cm^{-1} resolution with a FTIR spectrometer (Bruker Vertex 70) with a MIR light source using a 3.0 mm aperture, a CaF$_2$ beamsplitter and a LN-MCT detector with a scanning velocity of 80 kHz. The bandwidth was restricted to 5266 cm^{-1} and a 20 kHz acquisition filter with a low-pass cutoff at 3950 cm^{-1} was used. Spectra were averaged over 2000 scans at 12 K. The matrix was annealed by raising the temperature to 20, 25, and 30 K for 10 min each and finally 30 K again for 20 min, with a spectrum recorded after each annealing cycle. This allowed for diffusion of the

molecules within the Ar matrix promoting further cluster formation as well as relaxation of meta-stable matrix sites.[47−49]

COMPUTATIONAL DETAILS

Electronic structure calculations were performed with density functional theory (DFT) functionals B3LYP,[50] M06-2X,[51] PBE0,[52,53] and CAM-B3LYP[54] including the Grimme D3 empirical dispersion,[55] and ωB97X-D,[56] which includes the Grimme D2 empirical dispersion.[57] All DFT calculations were performed with Gaussian 16 using the aug-cc-pVTZ (AVTZ) basis set[58,59] and the "verytight" convergence criteria and the "ultrafine" integration grid.[60] A normal mode harmonic oscillator frequency calculation (NM HO) of the optimized geometries ensured convergence to a minimum. Finally, CCSD(T)-F12a/cc-pVDZ-F12 single-point energy calculations were performed on the ωB97X-D/AVTZ optimized geometries using Molpro12.1.[61−65]

A manual conformer search for alternative $(t\text{-BuOOH})_2$ structures was performed by varying the starting structure angles, dihedral angles, and number of hydrogen bonds and optimizing all generated structures at the ωB97X-D/AVTZ level of theory with the default optimization criteria in Gaussian 16. If a new conformer was found, it was reoptimized with the "verytight" convergence criteria and a NM HO calculation was performed.

The NCIs of the lowest energy optimized $(t\text{-BuOOH})_2$ structure was analyzed using NCIPLOT4.0 software.[40] The programme is used to calculate and visualize the reduced density gradient $s(\mathbf{r}) = 0.5$ a.u. isosurfaces[41−43] where $\mathbf{r}$ is a spatial coordinate. The surfaces are constructed from the CCSD(T)-F12a/cc-pVDZ-F12//ωB97X-D/AVTZ wave function using the "ultrafine" keyword for integration. The isosurfaces are color coded for the range -0.015 a.u. < sign$(\lambda_2)\cdot\rho(\mathbf{r})$ < 0.015 a.u. where λ_2 is the second eigenvalue of the electron density Hessian and $\rho(\mathbf{r})$ is the electron density.

The frequency and oscillator strength of the OH$_b$-stretching transition were calculated with a one-dimensional local mode model (1D LM) programmed in Python 3.[66] The potential energy surface (PES) was sampled along the OH bond displacement coordinate: $q = [-0.45; 1.475$ Å] in 0.025 Å increments from the ωB97X-D/AVTZ equilibrium geometry. The points were interpolated to $\Delta q = 0.00002$ Å using a cubic spline to ensure convergence within the used Simpson's integration method. The vibrational Schrödinger equation was solved in a basis of the first 50 associated Legendre $m = 1$ polynomials. The Cartesian components of the dipole moment function were sampled and interpolated in the same way along the coordinate q.

The unitless oscillator strength was calculated as[67,68]

$$f = 4.702 \cdot 10^{-7} \frac{\text{cm}}{D^2} \cdot \tilde{\nu}_{10} \cdot |\vec{\mu}_{10}|^2 \tag{3}$$

where $\tilde{\nu}_{10}$ is the transition wavenumber in cm^{-1} and $\vec{\mu}_{10}$ the transition dipole moment in Debye (1D = 3.33564×10^{-30} C·m). The oscillator strength can be converted to units of km/mol by the multiplication factor 5.3313×10^6 km/mol.

The coupling between the two OH-stretching oscillators in $(t\text{-BuOOH})_2$ was estimated using a two-dimensional (2D) harmonically coupled anharmonic oscillator LM (HCAO LM) model.[69,70] The 2D PES was sampled along the displacement coordinates of the two chemically equivalent oscillators: q_1, q_2 = $[-0.075; 0.075$ Å] in 0.025 Å increments around the ωB97X-D/AVTZ equilibrium geometry. The force constants

were determined by fitting the 7×7 PES grid to a 2D polynomial to the sixth order. The harmonic coupling was then estimated from the second-order force constants by[69,70]

$$\gamma' = -\frac{1}{2} \frac{F_{12}}{\sqrt{F_{11}}\sqrt{F_{22}}} \cdot \tilde{\omega} \tag{4}$$

where γ' is the coupling parameter, F_{ij} is the second-order derivative of the PES with respect to the displacement coordinates, $\tilde{\omega} = \sqrt{\frac{F_{11}}{\mu_{OH}}}/(2\pi c)$ is the harmonic transition wavenumber of the OH$_b$-stretch, and μ_{OH} is the reduced mass of the oscillator.

RESULTS AND DISCUSSION

Matrix Isolation FTIR Spectroscopy. Initially, we use matrix isolation FTIR spectra of t-BuOOH deposited in an Ar matrix to detect the formation of its clusters. Cold experiments give the optimal conditions for cluster formation as the entropic penalty of losing three vibrational and three rotational degrees of freedom upon cluster formation is minimized. In the top panel of Figure 1, we show the spectrum of the initial
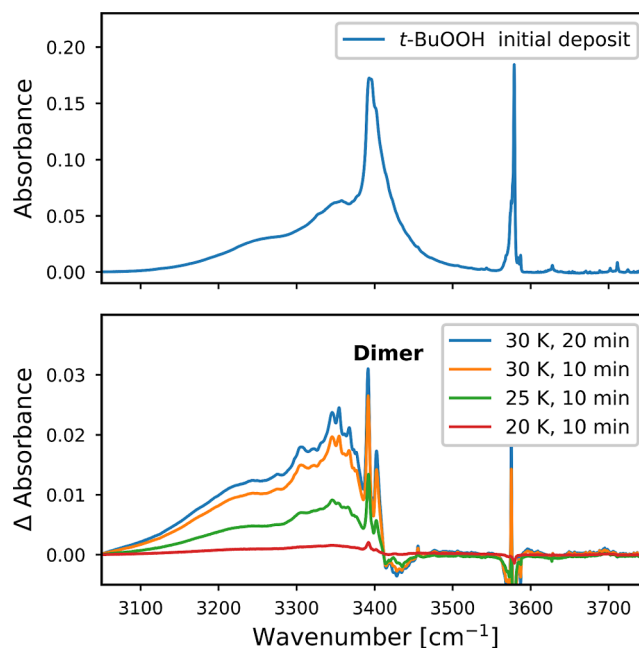

Figure 1. FTIR spectrum of t-BuOOH in a frozen Ar matrix. t-BuOOH is diluted 1:1790 in Ar and deposited on a CsI window at 12 K. Upper panel: spectrum immediately after the t-BuOOH/Ar mixture is deposited. Lower panel: difference spectra after each of the annealing cycles. Spectra are recorded between cycles and the initial deposit spectrum is subtracted.

deposited sample. An intense and narrow band from the OH-stretch in t-BuOOH monomer is observed at 3579 cm^{-1}. We assign the broader and stronger band at $\sim$3400 cm^{-1} to the OH$_b$-stretch of $(t\text{-BuOOH})_2$. A broad tail to lower wavenumbers is assigned as multiple OH$_b$-stretching bands of larger t-BuOOH clusters (multimers). In the bottom panel of Figure 1, we show the difference spectra after each annealing cycle with the initial deposit spectrum subtracted. In the difference spectra, the bands associated with $(t\text{-BuOOH})_2$ and larger clusters increase with each annealing cycle, while those of the monomer becomes increasingly negative as free monomer is

used to form the clusters. Two peaks associated with the dimer are observed to grow with each annealing cycle at 3392 and 3402 cm^{-1}, respectively. The appearance of two peaks is most probable due to the clusters getting trapped in different sites in the matrix with varying stabilization.[47−49] At 3628 cm^{-1}, the OH-stretching band from trace amounts of t-BuOH present in the sample can be seen. The minor sharp absorbance peaks at higher energies are from trace amounts of water in the sample compartment.

Theoretically, we identify five conformers of $(t\text{-BuOOH})_2$ (Section S16). The lowest energy conformer of $(t\text{-BuOOH})_2$ is shown to the left in Figure 2. The structure has a doubly
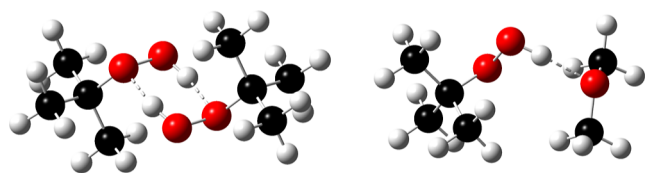

Figure 2. Calculated lowest energy ωB97X-D/AVTZ structures. Left: doubly hydrogen bound $(t\text{-BuOOH})_2$. Right: singly bound t-BuOOH· DME.

hydrogen bound six-membered ring in agreement with earlier findings for other hydroperoxide complexes.[23−29,31] At the ωB97X-D/AVTZ and B3LYP-D3/AVTZ levels of theory, all high-energy conformers have zero point corrected electronic formation energies, ΔE (ΔH at 0 K), that are 15−20 kJ/mol higher than the most stable conformer found, and Gibbs formation energies, ΔG, about 9−14 kJ/mol higher at 298 K (Table S6). This makes population of the high-energy conformers highly unlikely both in the matrix and the gas phase room temperature experiments. The difference, $\Delta H - \Delta G$, between the lowest energy conformer and the four other found conformers, highlights the entropic energy penalty of ca. 5 kJ/mol at 298 K associated with forming the rigid ring in the lowest energy structure. In the cold experiment, we find that formation of $(t\text{-BuOOH})_2$ is favored over that of larger clusters. Thus, in the gas phase at room temperature, clusters larger than the dimer are very unlikely to form. In contrast, alcohols have previously been reported to favor larger clusters.[71−74] The matrix isolation spectra show that formation of $(t\text{-BuOOH})_2$ is possible and provides an estimate of the OH-stretching redshift of ∼180 cm^{-1}.

Gas Phase Spectral Subtraction. In the gas phase, isolation of the $(t\text{-BuOOH})_2$ spectrum relies on accurate spectral subtraction of the t-BuOOH monomer, solvents, and impurities. Quantification of K relies on determination of the t-BuOOH monomer and dimer pressures. Within the approach we use, the measured integrated absorbance of the OH$_b$-stretching band and a calculated oscillator strength of the OH$_b$-stretching transition is used to determine the dimer pressure. We assume that the observed band only gains intensity from the OH$_b$-stretching transition in $(t\text{-BuOOH})_2$.

Due to its limited stability, t-BuOOH is commercially available only as solutions in decane and water, two solvents that are difficult to quantify and subtract from the measured spectrum of the gas mixture. For water, this is due to its rotational fine-structure, which is sensitive to pressure and temperature changes. For decane, it is due to its broad CH-stretching and HCH-bending bands, which overlap the bands from t-BuOOH. To avoid the challenge of quantifying these solvents in the gas mixture, we exchange the solvent to DCM.

DCM has a very clear and characteristic CH-stretching/HCH-bending combination band with visible rotational fine-structure centered at 4467 cm^{-1} that facilitate accurate spectral subtraction (Figure 3B). In addition, DCM absorbance
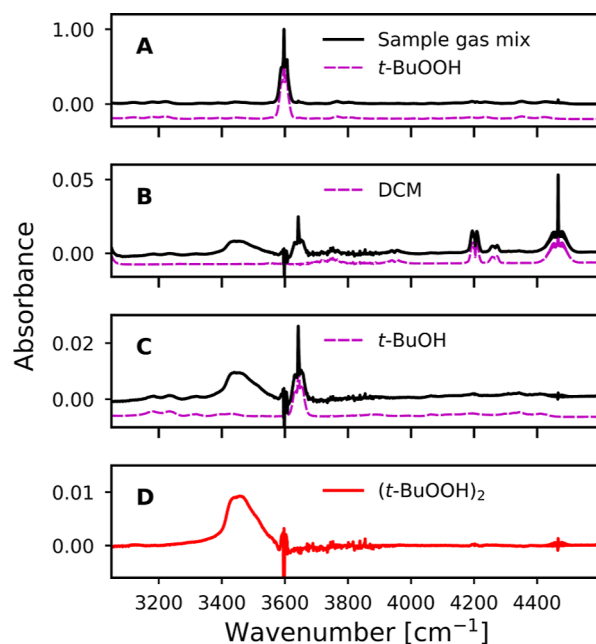
Figure 3. In panel A, the spectrum of the original sample is shown. In panel B, the t-BuOOH monomer has been subtracted leaving a spectrum of $(t\text{-BuOOH})_2$ with DCM and t-BuOH impurities. In panel C, we have subtracted DCM, and in panel D, t-BuOH has been subtracted, leaving a spectrum of pure $(t\text{-BuOOH})_2$. In frames A, B, and C, the reference spectrum of the largest impurity is shown with a dashed line underneath the spectrum of the sample gas mix.

bands are very weak in the OH-stretching region. The most prevalent impurity in the t-BuOOH sample, apart from the solvent, is its degradation product t-BuOH[75,76] with an OH-stretching band at 3643 cm^{-1} (Figure 3C). We record reference spectra of t-BuOH and DCM with known pressures and subtract these reference spectra from the sample mix spectra to estimate their respective partial pressures in the sample. This leaves a spectrum of only t-BuOOH + (t-BuOOH)$_2$ and gives an accurate estimate of the t-BuOOH monomer partial pressure as the partial pressure of the dimer is negligible. The t-BuOOH monomer pressure is corrected for the partial pressure contributions from the solvent and impurities to the total pressure.

In Figure 3, we show the progression from the initial sample spectrum to the final $(t\text{-BuOOH})_2$ spectrum by subtraction of t-BuOOH monomer-, DCM-, and t-BuOH reference spectra, respectively. The amount of t-BuOH and especially DCM that is subtracted varies significantly between the different experiments. The spectrum shown has a measured total sample pressure of 6.51 Torr. Reference spectra of DCM corresponding to 2.83 Torr and t-BuOH corresponding to 0.19 Torr is subtracted. This leaves a determined t-BuOOH monomer pressure of 3.49 Torr. The estimated pressure of $(t\text{-BuOOH})_2$ present in the sample is about 3 orders of magnitude smaller than that of the t-BuOOH monomer and can be ignored in the determination of the monomer pressure. Due to the low partial pressure of $(t\text{-BuOOH})_2$, its associated OH$_b$-stretching band is very weak in comparison to the OH-stretch of the t-BuOOH

monomer. This is noticeable in the change in absorbance-axis from panel A to the other panels. The spectra have been refined by subtracting the reference spectra of ambient water in the cell compartment of the spectrometer. We also correct for a slight ice build-up on the LN-MCT detector (Sections S5 and S6).

In the (t-BuOOH)$_2$ spectrum (Figure 3D), we observe small residuals from imperfect subtraction of the intense t-BuOOH monomer signal at around 3597 cm^{-1}. Small residual signals from DCM subtraction is also observed at 4467 cm^{-1} and finally signals from water impurities are observed in the region 3600−3950 cm^{-1}. This is primarily due to differences in pressure-broadening of the sharp rotational-vibrational lines between the spectra of the samples and the references. We also recorded spectra of the decane solvated t-BuOOH sample and obtained a spectrum of (t-BuOOH)$_2$ with a band profile indistinguishable to that of the DCM solvated sample (Section S11).

Band Shape and Position. In Figure 4, we show the OH$_b$-stretching band of (t-BuOOH)$_2$ measured for different t-
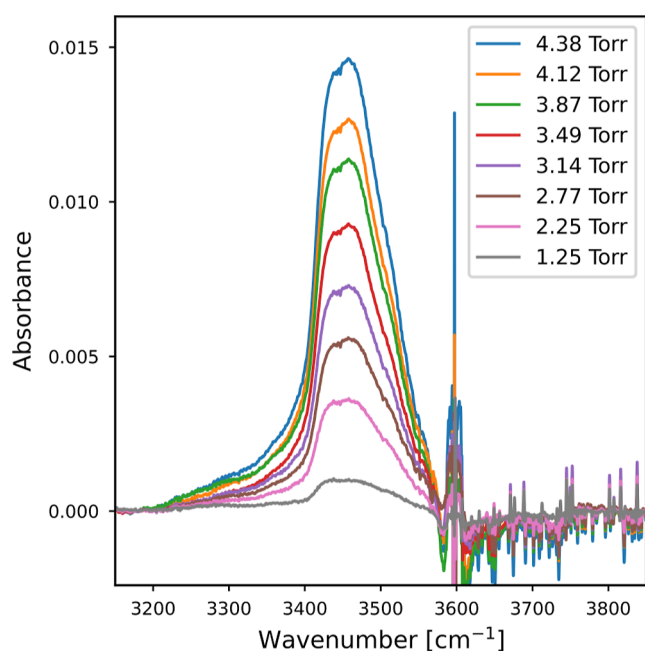
Figure 4. Subset of the recorded (t-BuOOH)$_2$ spectra. Labels denote t-BuOOH monomer pressure in each experiment.

BuOOH monomer pressures. The absorbance band is asymmetric with a full width at half maximum (fwhm) of ~110 cm^{-1}. The intensity-weighted center of the band is 3452 cm^{-1}, which corresponds to an OH-stretching band redshift of 145 cm^{-1} from the t-BuOOH monomer (Table 1). However,

the two OH$_b$-stretching modes in (t-BuOOH)$_2$ couple, leading to an IR-inactive symmetric transition and an IR-active antisymmetric transition, the latter of which gives rise to the observed band. The splitting of the two transitions are calculated to be 35 cm^{-1} with the HCAO LM model (32 cm^{-1} with NM HO model) with the antisymmetric transition at the highest energy. A decoupled OH$_b$-stretching transition would be located in between the symmetric/antisymmetric transitions or about 18 cm^{-1} lower than that observed. The coupling between the two modes thus attenuate the observed redshift. In addition, the maximum of the OH$_b$-stretching band in hydrogen bound complexes shift to higher wavenumbers as the temperature increases due to coupling and population of the low-frequency intermolecular modes. In methanol dimer, for example, the cold OH$_b$-stretching band is located at the onset of the warm OH$_b$-stretching band.[9,77] In general, the OH$_b$-stretching band maximum occurs ca. 25 cm^{-1} lower in cold spectra compared to the corresponding band maximum at room temperature. This is illustrated in a few examples for different hydrogen bound complexes.[9,73,77]

To experimentally decouple the two OH$_b$-stretching oscillators, we record spectra of a partially deuterated t-BuOOH sample. The sample is deuterated to roughly 50% atom D. Thus, the spectrum will contain a mix of dimers formed with either 0, 1, or 2H replaced by D, roughly in ratio 1:2:1. The formed t-BuOOH·t-BuOOD dimer is observed in both matrix experiments and in gas phase room temperature experiments. In the 12 K matrix isolation difference spectra of the partly deuterated sample (Figure S15), we determine a 17 cm^{-1} shift of the two observed OH$_b$-stretching bands in good agreement with the calculated shift expected from decoupling the two OH$_b$-stretching transitions. Due to temperature effects, the observed shift under cold conditions of ca. 17 cm^{-1} is a more direct measure of the decoupling of the two OH$_b$-stretching oscillators. If we include the additional shift of 17 cm^{-1}, the redshift of the isolated OH$_b$-stretching band in (t-BuOOH)$_2$ becomes 162 cm^{-1}, which is comparable to the 170 cm^{-1} redshift found for t-BuOOH·DME.[22]

In Figure 5, the OH$_b$-stretching band position in the gas phase spectrum of (t-BuOOH)$_2$ is compared to that of the partially deuterated dimer t-BuOOH·t-BuOOD. We subtract the spectrum of the non-deuterated dimer from the spectrum of the mixture to obtain the spectrum of the singly- and doubly deuterated dimers t-BuOOH·t-BuOOD and (t-BuOOD)$_2$. The latter is expected to have no intensity in the OH-stretching region. We observe an OH$_b$-stretching band maximum of t-BuOOH·t-BuOOD at ~3415 cm^{-1}, which is shifted ~37 cm^{-1} from the intensity weighted maximum of the non-deuterated (t-BuOOH)$_2$. The 37 cm^{-1} shift in the gas phase is ca. 20 cm^{-1} larger than that found in the matrix isolation experiment. We attribute the width and shape of the OH$_b$-stretching band of (t-

Table 1. Calculated ωB97X-D/AVTZ Geometric Parameters and Room-Temperature Observed Redshifts[a]

	$\theta_{OH\cdots O}$ [°]	$R_{OH\cdots O}$ [Å]	ΔR_{OH} [Å]	calc $\tilde{\nu}$	obs $\tilde{\nu}$[b]	obs $\Delta\tilde{\nu}$
t-BuOOH				3669[c]	3597	
(t-BuOOH)$_2$	154.2	1.90	0.0115	3413[c]	3452	145 (162)[f]
t-BuOOH·DME[d]	168.4	1.81	0.0123	3363[e]	3428	170
	163.1	1.83	0.0126	3356[e]		

[a]All $\tilde{\nu}$ are in units of cm^{-1}. [b]Band maximum. Intensity weighted band maximum for (t-BuOOH)$_2$. [c]Calculated with 1D LM model. [d]Values from Møller et al.[22] includes two conformers. [e]1D LM model assuming Morse potential from Møller et al.[22] [f]Redshift including the 17 cm^{-1} shift from decoupling the OH$_b$-stretch in the dimer.
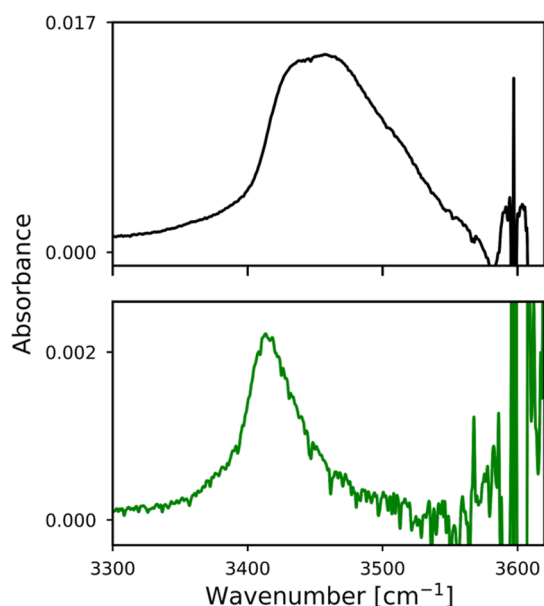
Figure 5. Gas-phase spectra at 298 K of non-deuterated $(t\text{-BuOOH})_2$ and partly deuterated $t\text{-BuOOH}\cdot t\text{-BuOOD}$. Top panel: the spectrum of the non-deuterated $(t\text{-BuOOH})_2$ at 4.38 Torr monomer pressure, equivalent to the highest trace in Figure 4. Bottom panel: the band associated with the OH_b-stretch in the singly deuterated dimer ($t\text{-BuOOH}\cdot t\text{-BuOOD}$). The spectrum is recorded at a measured total pressure of 4.7 Torr. The band has a maximum at 3415 cm^{-1}.

BuOOH)$_2$ to the coupling of the OH_b-stretching mode with the low frequency intermolecular modes. Previous studies of weakly hydrogen bound complexes have shown that the low frequency intermolecular modes can significantly widen and change the overall shape of the observed OH_b-stretching band at room temperature.[9,44,73,78,79] The OH_b-stretching transition occurs from a manifold of thermally populated low lying vibrational states, translating into many hot transitions that all contribute intensity to the observed band.[78] The band shape of $t\text{-BuOOH}\cdot t\text{-BuOOD}$ is more narrow with a fwhm ~45 cm^{-1}. This reduced width is likely due to changes in frequencies and population of the intermolecular modes upon deuteration. No clear combination bands are observed in the cold experiments and it is therefore unlikely that these will contribute significantly to the band at room temperature.

It is difficult to calculate accurately the frequencies and oscillator strengths of OH_b-stretching transitions in weakly bound complexes.[78,80−82] We use a 1D LM model to calculate the frequency and oscillator strength of the OH_b-stretching transitions in $(t\text{-BuOOH})_2$. In the 1D LM model, the OH_b-stretch is not coupled to the intermolecular modes and thus gives reasonable results for the OH_b-stretching transition with a minimum of variables. The 1D LM model predicts a transition wavenumber of 3413 cm^{-1} with ωB97X-D/AVTZ, which is fairly close to the observed band maximum. The simplistic 1D LM model overestimates the redshift of the OH_b-stretch due to the omission of coupling to the low frequency intermolecular modes.[82,83]

In Table 1, the calculated geometric parameters and redshifts are compared with the observed redshifts for $(t\text{-BuOOH})_2$ and for the bi-molecular complex $t\text{-BuOOH}\cdot\text{DME}$ (Figure 2, Right). Smaller hydrogen bond angles, smaller elongation of O−H intramolecular bonds and longer hydrogen bonds are all indicative of weaker hydrogen bonds in $(t\text{-}$

BuOOH)$_2$ compared to $t\text{-BuOOH}\cdot\text{DME}$.[10,11] The slightly smaller redshift in $(t\text{-BuOOH})_2$ compared to that in $t\text{-BuOOH}\cdot\text{DME}$ also suggests weaker individual OOH···O hydrogen bonds in $(t\text{-BuOOH})_2$. The ring strain in the $(t\text{-BuOOH})_2$ structure leads to non-optimal hydrogen bond angles of 154.2°, smaller than that found in $t\text{-BuOOH}\cdot\text{DME}$ and is in line with the smaller redshift.

Constant of Dimer Formation. To determine the constant of dimer formation, the amount of $(t\text{-BuOOH})_2$ present in the gas mixture must be determined. The $(t\text{-BuOOH})_2$ partial pressure is determined from eq 2, where the OH_b-stretching band is integrated between 3250 and 3577 cm^{-1}. We estimate the theoretical oscillator strength (f_{calc}) of the entire OH_b-stretching band in $(t\text{-BuOOH})_2$ to be 1.4 × 10^{-4}. This arises from two times the oscillator strength of one OH_b-stretching transition, which is calculated with the 1D LM model to be 9.1 × 10^{-5} (ωB97X-D/AVTZ) and empirically corrected for the effect of the coupling to the intermolecular modes.[83] The empirical correction comes from a relatively robust discrepancy found between the 1D LM model and a LM perturbation theory model, which includes coupling to the intermolecular modes. The two models were applied to a range of hydrogen bound complexes, for which a reduction in intensity of ~25% was observed when introducing coupling to the intermolecular modes.[81−83]

In Figure 6, the estimated pressure of $(t\text{-BuOOH})_2$ is fitted to the square of the $t\text{-BuOOH}$ monomer pressure for a number
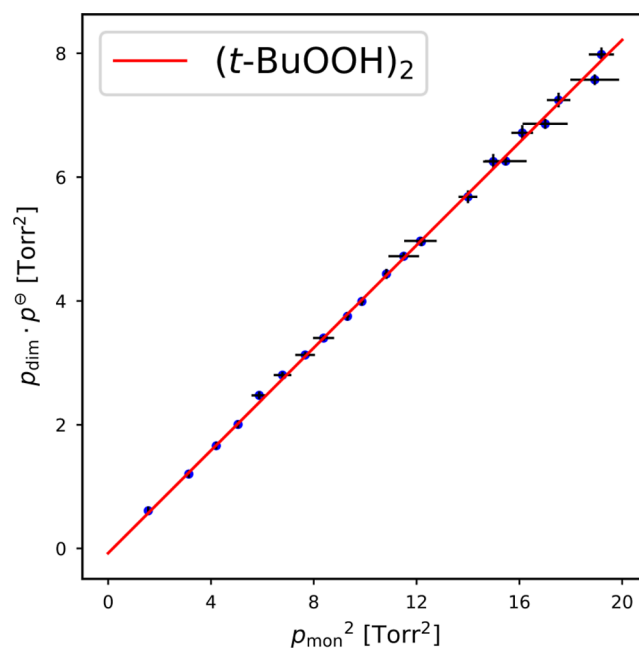
Figure 6. Determined $(t\text{-BuOOH})_2$ pressure fitted against $t\text{-BuOOH}$ monomer pressure squared. The linear fit is performed by minimizing a χ^2 taking into consideration the error on each individual measurement. The error bars indicate errors in monomer pressure and integrated absorbance in the horizontal and vertical direction, respectively.

of experiments. The determined monomer- and dimer pressures for all measurements are shown in Table S1. The constant of dimer formation for $(t\text{-BuOOH})_2$ is estimated to be $K = 0.41 \pm 0.017$ following eq 1, with the uncertainty reported as one standard error (σ_{std}) including all experimental errors. The statistical χ^2-fit uncertainty is 0.0054 and reflects a

Table 2. Equilibrium Constants and ΔG-Values at Room Temperature

	K	ΔG [kJ/mol]	T [K]	refs
$(t\text{-BuOOH})_2{}^a$	0.41	2.2	298	this work
$t\text{-BuOOH·DME}^a$	0.17	4.4	295–298	Møller et al.[22]
$t\text{-BuOH·DME}^a$	0.031	8.6	295–298	Møller et al.[22]
$(t\text{-BuOOH})_2{}^b$	1.90	−1.6	303	Walling & Heaton[30]
$(t\text{-BuOOD})_2{}^b$	1.65	−1.3	303	Walling & Heaton[30]
$(\text{CH}_3\text{COOH})_2$	[30, 2000]	[−8,−18]		various sources.[17,19−21]
$\text{CH}_3\text{COOH·MeOH}^a$	1.1	−0.24	308	Wagner et al.[39]

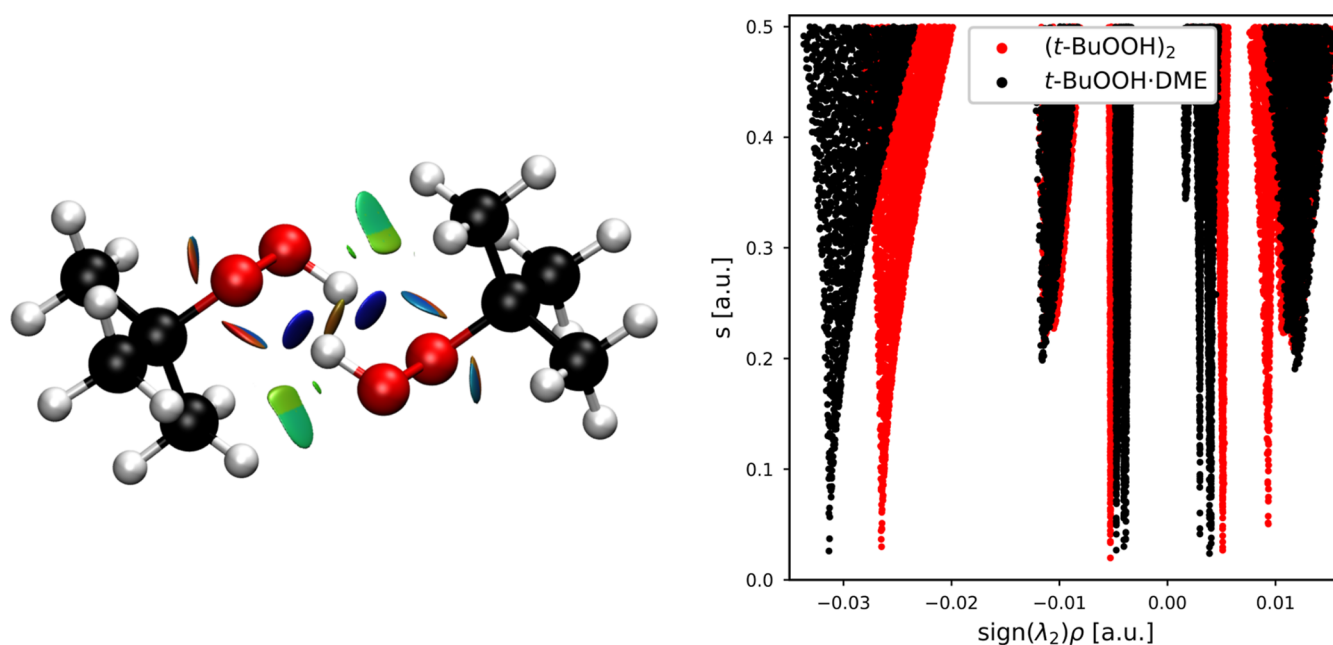^{a}Gas-phase experiment. ^{b}In solution of CCl$_4$.

Figure 7. NCI analyses of $(t\text{-BuOOH})_2$. Left: the NCI $s(\mathbf{r}) = 0.5$ a.u. isosurfaces in $(t\text{-BuOOH})_2$. Right: the $s(\mathbf{r})$ plotted vs $\text{sign}(\lambda_2)\cdot\rho(\mathbf{r})$ for $(t\text{-BuOOH})_2$ (red) and $t\text{-BuOOH·DME}$ (black).

very certain quadratic correlation between the integrated absorbance of the OH$_b$-stretching band and the monomer pressure as is expected for dimer formation. The quadratic correlation further rules out significant intensity contribution from a t-BuOOH trimer, which would introduce a cubic correlation between the integrated absorbance and the t-BuOOH monomer pressure. The $K = 0.41$ corresponds to a $\Delta G = 2.2$ kJ/mol at 298 K. The accuracy of the quantification of K is limited by the estimated oscillator strength, which we expect to be accurate to better than a factor of 2. K is inversely proportional to f_{calc} and ΔG scales logarithmically with K. Thus, we expect an accuracy of K to be within a factor 2 corresponding to an accuracy of ΔG of better than ± 1.7 kJ/mol at 298 K.

We also calculated ΔG directly with different DFT functionals within the harmonic oscillator and rigid rotor approximations. The difference between the ωB97X-D and B3LYP-D3 functionals are 2.9 kJ/mol corresponding to a factor 3.2 difference in K, underlining the sensitivity to the electronic structure method used in the purely theoretical approach (Table S10). In comparison, the calculated 1D LM oscillator strength of the OH$_b$-stretch, and by extension K, varies less than 20% between the ωB97X-D and the B3LYP-D3 methods (Section S12). This insensitivity of f_{calc} to electronic structure method is in agreement with results for other hydrogen bound complexes.[9] For example, the f_{calc} of the OH$_b$-

stretch varies less than 10% between the ωB97X-D and CCSD(T)-F12a methods for the MeOH·DMA complex. Thus, K determined with this hybrid method is relatively insensitive to the choice of the electronic structure method.

In Table 2, we compare K for various hydrogen bound complexes and dimers. The experimentally determined constant of dimer formation and corresponding ΔG value at 298 K for t-BuOOH·DME is 0.17 and 4.4 kJ/mol, respectively. $(t$-BuOOH$)_2$ thus has an increased stabilization of ca. 2.2 kJ/mol at 298 K compared to t-BuOOH·DME. The modest increase in stabilization was surprising, as we expected the binding-enthalpy from forming an additional hydrogen bond to shift the ΔG value significantly. This phenomenon is observed for carboxylic acids, where constants of dimer formation of the doubly bound dimers are orders of magnitude larger than that of the singly bound complexes. For acetic acid, the constants of dimer formation of the singly hydrogen bound complexes with methanol and ethanol were experimentally estimated to $K \sim 1$.[39] The fluorinated version, trifluoroacetic acid, also forms complexes with various ketones with $K < 1$.[84] However, upon forming two hydrogen bonds in an eight-membered ring in an acetic acid dimer, theoretical studies report $K \sim 30-860$[17] and IR-, NMR-, and vapor density experiments estimate values in the order of $K \sim 1000-2000$.[19−21] For formic acid with a similar eight-membered ring, K is estimated from theory and experiments in the order of ~ 300.[12−16] In $(t$-BuOOH$)_2$, the

weakening of the individual hydrogen bonds, as well as an additional entropic energy penalty from forming a rigid ring, results in the modest additional stabilization of ca. 2.2 kJ/mol at room temperature. Previously, K has been determined for (t-BuOOH)$_2$ and (t-BuOOD)$_2$ in CCl$_4$ solution to be 1.90 and 1.65, respectively.[30] These values are significantly higher than the gas-phase value presented here. In the CCl$_4$ experiment, the reported K is lower for the deuterated dimer, which is opposing the common trend of deuterated species forming stronger bound complexes.[85]

In Figure 7, we show the NCI analysis of the intermolecular electron densities and the reduced electron density gradients. To the left is shown the spatial analysis illustrated as $s(\mathbf{r}) = 0.5$ a.u. isosurfaces and to the right the $s(\mathbf{r})$ is plotted versus sign(λ_2)·$\rho(\mathbf{r})$. The isosurfaces to the left are on a color gradient from strong attractive (blue) to weak secondary (green) to strong repulsive interactions (red). The hydrogen bonds are clearly visible as two deep blue-colored circular surfaces located close to the hydrogen atoms of each OOH group. In the 2D plot to the right, the $s(\mathbf{r})$ minima corresponding to the hydrogen bonds are located at sign(λ_2)·$\rho(\mathbf{r})$ = −0.0265 a.u. and −0.0313 a.u. for (t-BuOOH)$_2$ and t-BuOOH·DME, respectively, signifying weaker individual hydrogen bonds in (t-BuOOH)$_2$. An additional interaction in (t-BuOOH)$_2$, which is not present in the t-BuOOH·DME, is the repulsive interaction in the middle of the ring. This is seen as a red-brown isosurface in the center of (t-BuOOH)$_2$ and corresponds to the $s(\mathbf{r})$ extremum at sign(λ_2)·$\rho(\mathbf{r})$ = 0.0093 a.u. in the 2D plot.

CONCLUSIONS

We have detected (t-BuOOH)$_2$ in the gas phase at room temperature from its fundamental OH$_b$-stretching band. The band profile is wide and asymmetric with an intensity weighted maximum at 3452 cm^{-1}. We decoupled the two OH-stretching oscillators by partially deuterating the dimer. This facilitated direct comparison with the redshift of the singly bound t-BuOOH·DME complex which was found to be similar to that of (t-BuOOH)$_2$. The matrix isolation spectrum of t-BuOOH·t-BuOOD dimer provided an estimate of the HCAO LM coupling parameter, γ', of 17 cm^{-1} between the two OH$_b$-stretching vibrations. The calculated lowest energy structure of the dimer is a closed 6-membered ring structure, which imposes non-optimal angles for the hydrogen bonds. Other conformers were found energetically unfavorable and were not detected at room temperature. The constant of dimer formation is determined to be ∼0.4, which is roughly twice that found for the singly bound t-BuOOH·DME complex. This rough factor two increase from a singly to a doubly hydrogen bound complex is significantly smaller than that found for carboxylic acids.

ASSOCIATED CONTENT

Ⓢ Supporting Information

The Supporting Information is available free of charge at https://pubs.acs.org/doi/10.1021/acs.jpca.3c03702.

Protocol of the t-BuOOH sample phase extracted from H$_2$O into DCM; H-NMR and C-NMR spectra of finished samples confirming purity and estimating residual DCM and H$_2$O content; measured and estimated pressures of all experiments; spectral refinement by subtracting water vapor- and ice signals from

the spectra; details on baseline corrections and integration limits; estimation of experimental errors and procedure of propagation of error; data treatment of commercially available t-BuOOH solvated in decane; oscillator strengths and transition wavenumbers calculated with different models for t-BuOOH and (t-BuOOH)$_2$; deuteration of t-BuOOH sample is shown and the 12 K matrix spectra of the partly deuterated sample; integrated kinetic energy densities $G(s_{0.5})$ of the NCI analyses; alternative conformers found and thermodynamic properties; Mulliken charge distributions in the t-BuOOH monomer, dimer, and the t-BuOOH·DME complex; and calculated thermodynamic properties for the most stable conformer are reported with different DFT functionals (PDF)

AUTHOR INFORMATION

Corresponding Author

Henrik G. Kjaergaard − *Department of Chemistry, University of Copenhagen, 2100 Copenhagen-Ø, Denmark;* ○ orcid.org/0000-0002-7275-8297; Phone: +45 35320334; Email: hgk@chem.ku.dk; Fax: +45 35320322

Author

Casper Vindahl Jensen − *Department of Chemistry, University of Copenhagen, 2100 Copenhagen-Ø, Denmark;* ○ orcid.org/0000-0002-9102-1223

Complete contact information is available at:
https://pubs.acs.org/10.1021/acs.jpca.3c03702

Notes

The authors declare no competing financial interest.

REFERENCES

(1) Hubbard, R. E.; Haider, M. K. Hydrogen Bonds in Proteins: Role and Strength. In *Encyclopedia of Life Sciences (ELS)*; John Wiley & Sons, Ltd, 2010.

(2) Ippolito, J. A.; Alexander, R. S.; Christianson, D. W. Hydrogen Bond Stereochemistry in Protein Structure and Function. *J. Mol. Biol.* **1990**, *215*, 457−471.

(3) Hooft, R. W.; Sander, C.; Vriend, G. Positioning Hydrogen Atoms by Optimizing Hydrogen-Bond Networks in Protein structures. *Proteins: Struct., Funct., Bioinf.* **1996**, *26*, 363−376.

(4) McDonald, I. K.; Thornton, J. M. Satisfying Hydrogen Bonding Potential in Proteins. *J. Mol. Biol.* **1994**, *238*, 777−793.

(5) Creighton, T. E. Stability of Folded Conformations: Current Opinion in Structural Biology 1991, 1: 5−16. *Curr. Opin. Struct. Biol.* **1991**, *1*, 5−16.

(6) Bianchi, F.; Kurtén, T.; Riva, M.; Mohr, C.; Rissanen, M. P.; Roldin, P.; Berndt, T.; Crounse, J. D.; Wennberg, P. O.; Mentel, T. F.; et al. Highly Oxygenated Organic Molecules (HOM) from Gas-Phase Autoxidation involving Peroxy Radicals: A Key Contributor to Atmospheric Aerosol. *Chem. Rev.* **2019**, *119*, 3472−3509.

(7) Zhang, R.; Khalizov, A.; Wang, L.; Hu, M.; Xu, W. Nucleation and Growth of Nanoparticles in the Atmosphere. *Chem. Rev.* **2012**, *112*, 1957−2011.

(8) Zhao, J.; Khalizov, A.; Zhang, R.; McGraw, R. Hydrogen-Bonding Interaction in Molecular Complexes and Clusters of Aerosol Nucleation Precursors. *J. Phys. Chem. A* **2009**, *113*, 680−689.

(9) Hansen, A. S.; Vogt, E.; Kjaergaard, H. G. Gibbs Energy of Complex Formation−Combining Infrared Spectroscopy and Vibrational Theory. *Int. Rev. Phys. Chem.* **2019**, *38*, 115−148.

(10) Arunan, E.; Desiraju, G. R.; Klein, R. A.; Sadlej, J.; Scheiner, S.; Alkorta, I.; Clary, D. C.; Crabtree, R. H.; Dannenberg, J. J.; Hobza, P.; et al. Defining the Hydrogen Bond: An account (IUPAC Technical Report). *Pure Appl. Chem.* **2011**, *83*, 1619−1636.

(11) Arunan, E.; Desiraju, G. R.; Klein, R. A.; Sadlej, J.; Scheiner, S.; Alkorta, I.; Clary, D. C.; Crabtree, R. H.; Dannenberg, J. J.; Hobza, P.; et al. Definition of the Hydrogen Bond (IUPAC Recommendations 2011). *Pure Appl. Chem.* **2011**, *83*, 1637−1641.

(12) Mackeprang, K.; Xu, Z.-H.; Maroun, Z.; Meuwly, M.; Kjaergaard, H. G. Spectroscopy and Dynamics of Double Proton Transfer in Formic Acid Dimer. *Phys. Chem. Chem. Phys.* **2016**, *18*, 24654−24662.

(13) Barton, J. R.; Hsu, C. PVTX Properties of Associated Vapors of Formic and Acetic Acids. *J. Chem. Eng. Data* **1969**, *14*, 184−187.

(14) Vander Auwera, J.; Didriche, K.; Perrin, A.; Keller, F. Absolute Line Intensities for Formic Acid and Dissociation Constant of the Dimer. *J. Chem. Phys.* **2007**, *126*, 124311.

(15) Winkler, A.; Hess, P. Study of the Energetics and Dynamics of Hydrogen Bond Formation in Aliphatic Carboxylic Acid Vapors by Resonant Photoacoustic Spectroscopy. *J. Am. Chem. Soc.* **1994**, *116*, 9233−9240.

(16) Miyamoto, S.; Nakamura, S.; Iwai, Y.; Arai, Y. Measurement of Vapor-Phase Compressibility Factors of Monocarboxylic Acids using a Flow-Type Apparatus and their Association Constants. *J. Chem. Eng. Data* **1999**, *44*, 48−51.

(17) Colominas, C.; Teixidó, J.; Cemelí, J.; Luque, F. J.; Orozco, M. Dimerization of Carboxylic Acids: Reliability of Theoretical Calculations and the Effect of Solvent. *J. Phys. Chem. B* **1998**, *102*, 2269−2276.

(18) Chocholoušová, J.; Vacek, J.; Hobza, P. Acetic Acid Dimer in the Gas Phase, Nonpolar Solvent, Microhydrated Environment, and Dilute and Concentrated Acetic Acid: Ab Initio Quantum Chemical and Molecular Dynamics Simulations. *J. Phys. Chem. A* **2003**, *107*, 3086−3092.

(19) Togeas, J. B. Acetic Acid Vapor: 2. A Statistical Mechanical Critique of Vapor Density Experiments. *J. Phys. Chem. A* **2005**, *109*, 5438−5444.

(20) Goubet, M.; Soulard, P.; Pirali, O.; Asselin, P.; Réal, F.; Gruet, S.; Huet, T. R.; Roy, P.; Georges, R. Standard Free Energy of the Equilibrium between the Trans-Monomer and the Cyclic-Dimer of Acetic Acid in the Gas Phase from Infrared Spectroscopy. *Phys. Chem. Chem. Phys.* **2015**, *17*, 7477−7488.

(21) Socha, O.; Dračínský, M. Dimerization of Acetic Acid in the Gas Phase—NMR Experiments and Quantum-Chemical Calculations. *Molecules* **2020**, *25*, 2150.

(22) Møller, K. H.; Tram, C. M.; Kjaergaard, H. G. Side-by-Side Comparison of Hydroperoxide and Corresponding Alcohol as Hydrogen-Bond Donors. *J. Phys. Chem. A* **2017**, *121*, 2951−2959.

(23) Giguère, P. A.; Srinivasan, T. Raman Study of Matrix Isolated H₂O₂ and D₂O₂. *Chem. Phys. Lett.* **1975**, *33*, 479−482.

(24) Giguere, P. A. Intermediates in the Gas-Phase Disproportionation of HO₂ Radicals. *J. Phys. Chem.* **1981**, *85*, 3733−3734.

(25) Diem, M.; Tso, T.-L.; Lee, E. K. On the Bonding and Structure in Dihydroperoxyl (HO₂)₂ and H₂O₄. *J. Chem. Phys.* **1982**, *76*, 6452−6454.

(26) Dobado, J.; Molina, J. M. Ab Initio Molecular Orbital Calculation of the Hydrogen Peroxide Dimer: Study of Basis set Superposition Error. *J. Phys. Chem.* **1993**, *97*, 7499−7504.

(27) Engdahl, A.; Nelander, B.; Karlström, G. A Matrix Isolation and Ab Initio Study of the Hydrogen Peroxide Dimer. *J. Phys. Chem. A* **2001**, *105*, 8393−8398.

(28) Engdahl, A.; Nelander, B. The HOOH−HOO Complex. A Matrix Isolation Study. *Phys. Chem. Chem. Phys.* **2004**, *6*, 730−734.

(29) Qu, Y.; Bian, X.; Zhou, Z.; Gao, H. Existence of Hydroperoxy and Hydrogen Peroxide Radical Complex (HO₂ ·H₂O₂). *Chem. Phys. Lett.* **2002**, *366*, 260−266.

(30) Walling, C.; Heaton, L. Hydrogen Bonding and Complex Formation in Solutions of t-Butyl Hydroperoxide. *J. Am. Chem. Soc.* **1965**, *87*, 48−51.

(31) Duh, Y.-S.; Kao, C.-S.; Hwang, H.-H.; Lee, W. W.-L. Thermal Decomposition Kinetics of Cumene Hydroperoxide. *Process Saf. Environ. Prot.* **1998**, *76*, 271−276.

(32) Hansen, A. S.; Huchmala, R. M.; Vogt, E.; Boyer, M. A.; Bhagde, T.; Vansco, M. F.; Jensen, C. V.; Kjærsgaard, A.; Kjaergaard, H. G.; McCoy, A. B.; et al. Coupling of Torsion and OH-Stretching in tert-Butyl Hydroperoxide. I. The Cold and Warm First OH-Stretching Overtone Spectrum. *J. Chem. Phys.* **2021**, *154*, 164306.

(33) Vogt, E.; Huchmala, R. M.; Jensen, C. V.; Boyer, M. A.; Wallberg, J.; Hansen, A. S.; Kjærsgaard, A.; Lester, M. I.; McCoy, A. B.; Kjaergaard, H. G. Coupling of Torsion and OH-Stretching in tert-Butyl Hydroperoxide. II. The OH-Stretching Fundamental and Overtone Spectra. *J. Chem. Phys.* **2021**, *154*, 164307.

(34) Chandler, D. W.; Farneth, W. E.; Zare, R. N. A Search for Mode-Selective Chemistry: The Unimolecular Dissociation of t-Butyl Hydroperoxide Induced by Vibrational Overtone Excitation. *J. Chem. Phys.* **1982**, *77*, 4447−4458.

(35) Likar, M.; Baggott, J.; Crim, F. Vibrationally Mediated Photodissociation of t-Butyl Hydroperoxide: Vibrational Overtone Spectroscopy and Photodissociation Dynamics. *J. Chem. Phys.* **1989**, *90*, 6266−6274.

(36) Homitsky, S. C.; Dragulin, S. M.; Haynes, L. M.; Hsieh, S. O−H Stretch Overtone Excitation in Methyl and Ethyl Hydroperoxides. *J. Phys. Chem. A* **2004**, *108*, 9492−9499.

(37) Chuang, M.-C.; Baggott, J. E.; Chandler, D. W.; Farneth, W. E.; Zare, R. N. Unimolecular Decomposition of t-Butylhydroperoxide by Direct Excitation of the 6−0 O—H Stretching Overtone. *Faraday Discuss. Chem. Soc.* **1983**, *75*, 301−313.

(38) Baasandorj, M.; Papanastasiou, D. K.; Talukdar, R. K.; Hasson, A. S.; Burkholder, J. B. (CH₃)₃COOH (tert-Butyl Hydroperoxide): OH Reaction Rate Coefficients between 206 and 375 K and the OH Photolysis Quantum Yield at 248 nm. *Phys. Chem. Chem. Phys.* **2010**, *12*, 12101−12111.

(39) Wagner, M.; Apelblat, A.; Tamir, A. Excess Gibbs Free Energy in Methanol + Acetic Acid and Ethanol + Acetic Acid. *J. Chem. Thermodyn.* **1980**, *12*, 181−186.

(40) Contreras-García, J.; Johnson, E. R.; Keinan, S.; Chaudret, R.; Piquemal, J.-P.; Beratan, D. N.; Yang, W. NCIPLOT: A Program for Plotting Noncovalent Interaction Regions. *J. Chem. Theory Comput.* **2011**, *7*, 625−632.

(41) Johnson, E. R.; Keinan, S.; Mori-Sánchez, P.; Contreras-García, J.; Cohen, A. J.; Yang, W. Revealing Noncovalent Interactions. *J. Am. Chem. Soc.* **2010**, *132*, 6498−6506.

(42) Boto, R. A.; Contreras-García, J.; Tierny, J.; Piquemal, J.-P. Interpretation of the Reduced Density Gradient. *Mol. Phys.* **2016**, *114*, 1406−1414.

(43) Laplaza, R.; Peccati, F.; Boto, A.; Quan, C.; Carbone, A.; Piquemal, J.-P.; Maday, Y.; Contreras-García, J. NCIPLOT and the Analysis of Noncovalent Interactions using the Reduced Density Gradient. *Wiley Interdisc. Rev.: Comput. Mol. Sci.* **2021**, *11*, No. e1497.

(44) Hippler, M. Quantum Chemical Study and Infrared Spectroscopy of Hydrogen-Bonded CHCl₃−NH₃ in the Gas Phase. *J. Chem. Phys.* **2007**, *127*, 084306.

(45) Kjaergaard, H. G.; Low, G. R.; Robinson, T. W.; Howard, D. L. Calculated OH-Stretching Vibrational Transitions in the Water-Nitrogen and Water-Oxygen Complexes. *J. Phys. Chem. A* **2002**, *106*, 8955−8962.

(46) Hippler, M.; Hesse, S.; Suhm, M. A. Quantum-Chemical Study and FTIR Jet Spectroscopy of $CHCl_3$−NH_3 Association in the Gas Phase. *Phys. Chem. Chem. Phys.* **2010**, *12*, 13555−13565.

(47) Redington, R. L. Matrix Trapping Sites and Interactions with LiF Monomer. *J. Chem. Phys.* **1995**, *102*, 7332−7340.

(48) Kappe, C. O.; Wong, M. W.; Wentrup, C. Acetylketene: Conformational Isomerism and Photochemistry. Matrix Isolation Infrared and Ab Initio Studies. *J. Org. Chem.* **1995**, *60*, 1686−1695.

(49) Barnes, A. Matrix Isolation Vibrational Spectroscopy as a Tool for Studying Conformational Isomerism. *J. Mol. Struct.* **1984**, *113*, 161−174.

(50) Becke, A. Density-Functional Thermochemistry. III. The Role of Exact Exchange. *J. Chem. Phys.* **1993**, *98*, 5648−5652.

(51) Zhao, Y.; Truhlar, D. G. The M06 Suite of Density Functionals for Main Group Thermochemistry, Thermochemical Kinetics, Noncovalent Interactions, Excited States, and Transition Elements: Two New Functionals and Systematic Testing of Four M06-Class Functionals and 12 other Functionals. *Theor. Chem. Acc.* **2008**, *120*, 215−241.

(52) Adamo, C.; Barone, V. Toward Reliable Density Functional Methods Without Adjustable Parameters: The PBE0 Model. *J. Chem. Phys.* **1999**, *110*, 6158−6170.

(53) Ernzerhof, M.; Scuseria, G. E. Assessment of the Perdew−Burke−Ernzerhof Exchange-Correlation Functional. *J. Chem. Phys.* **1999**, *110*, 5029−5036.

(54) Yanai, T.; Tew, D. P.; Handy, N. C. A New Hybrid Exchange−Correlation Functional using the Coulomb-Attenuating Method (CAM-B3LYP). *Chem. Phys. Lett.* **2004**, *393*, 51−57.

(55) Grimme, S.; Antony, J.; Ehrlich, S.; Krieg, H. A Consistent and Accurate Ab Initio Parametrization of Density Functional Dispersion Correction (DFT-D) for the 94 Elements H-Pu. *J. Chem. Phys.* **2010**, *132*, 154104.

(56) Chai, J.-D.; Head-Gordon, M. Long-Range Corrected Hybrid Density Functionals with Damped Atom−Atom Dispersion Corrections. *Phys. Chem. Chem. Phys.* **2008**, *10*, 6615−6620.

(57) Grimme, S. Semiempirical GGA-Type Density Functional Constructed with a Long-Range Dispersion Correction. *J. Comput. Chem.* **2006**, *27*, 1787−1799.

(58) Dunning, T. H., Jr Gaussian Basis Sets for use in Correlated Molecular Calculations. I. The Atoms Boron through Neon and Hydrogen. *J. Chem. Phys.* **1989**, *90*, 1007−1023.

(59) Kendall, R. A.; Dunning, T. H., Jr; Harrison, R. J. Electron Affinities of the First-Row Atoms Revisited. Systematic Basis Sets and Wave Functions. *J. Chem. Phys.* **1992**, *96*, 6796−6806.

(60) Frisch, M. J.; Trucks, G. W.; Schlegel, H. B.; Scuseria, G. E.; Robb, M. A.; Cheeseman, J. R.; Scalmani, G.; Barone, V.; Petersson, G. A.; Nakatsuji, H. et al. *Gaussian 16*, Revision C.01.; Gaussian Inc: Wallingford CT, 2016.

(61) Adler, T. B.; Knizia, G.; Werner, H.-J. A Simple and Efficient CCSD(T)-F12 Approximation. *J. Chem. Phys.* **2007**, *127*, 221106.

(62) Peterson, K. A.; Adler, T. B.; Werner, H.-J. Systematically Convergent Basis Sets for Explicitly Correlated Wavefunctions: The Atoms H, He, B−Ne, and Al−Ar. *J. Chem. Phys.* **2008**, *128*, 084102.

(63) Werner, H.-J.; Knowles, P. J.; Celani, P.; Györffy, W.; Hesselmann, A.; Kats, D.; Knizia, G.; Köhn, A.; Korona, T.; Kreplin, D.; et al. MOLPRO, 12.1, a package of ab initio programs. URL visited July 2023. https://www.molpro.net (accessed July 12, 2023).

(64) Werner, H.-J.; Knowles, P. J.; Knizia, G.; Manby, F. R.; Schütz, M. Molpro: a General-Purpose Quantum Chemistry Program Package. *Wiley Interdiscip. Rev.: Comput. Mol. Sci.* **2012**, *2*, 242−253.

(65) Werner, H.-J.; Knowles, P. J.; Manby, F. R.; Black, J. A.; Doll, K.; Heßelmann, A.; Kats, D.; Köhn, A.; Korona, T.; Kreplin, D. A.; et al. The Molpro Quantum Chemistry Package. *J. Chem. Phys.* **2020**, *152*, 144107.

(66) Jensen, C. V. GitHub Repository of 1D LM code. URL visited July 2023. https://github.com/CasperVJensen/tert-Butyl_Hydroperoxide_Dimer.git (accessed July 12, 2023).

(67) Kjaergaard, H. G.; Yu, H.; Schattka, B. J.; Henry, B. R.; Tarr, A. W. Intensities in Local Mode Overtone Spectra: Propane. *J. Chem. Phys.* **1990**, *93*, 6239−6248.

(68) Atkins, P. W.; Friedman, R. S. *Molecular Quantum Mechanics*; Oxford University Press, 2011.

(69) Vogt, E.; Hansen, A. S.; Kjaergaard, H. G. *Molecular Spectroscopy: A Quantum Chemistry Approach*; Ozaki, Y., Wójcik, M. J., Popp, J., Eds.; John Wiley & Sons, 2019; Chapter 14, pp 289−424.

(70) Kjaergaard, H. G.; Garden, A. L.; Chaban, G. M.; Gerber, R. B.; Matthews, D. A.; Stanton, J. F. Calculation of Vibrational Transition Frequencies and Intensities in Water Dimer: Comparison of Different Vibrational Approaches. *J. Phys. Chem. A* **2008**, *112*, 4324−4335.

(71) Zimmermann, D.; Häber, T.; Schaal, H.; Suhm, M. A. Hydrogen Bonded Rings, Chains and Lassos: The Case of t-Butyl Alcohol Clusters. *Mol. Phys.* **2001**, *99*, 413−425.

(72) Hansen, A. S.; Du, L.; Kjaergaard, H. G. Positively Charged Phosphorus as a Hydrogen Bond Acceptor. *J. Phys. Chem. Lett.* **2014**, *5*, 4225−4231.

(73) Häber, T.; Schmitt, U.; Suhm, M. A. FTIR-Spectroscopy of Molecular Clusters in Pulsed Supersonic Slit-Jet Expansions. *Phys. Chem. Chem. Phys.* **1999**, *1*, 5573−5582.

(74) Larsen, R. W.; Zielke, P.; Suhm, M. A. Hydrogen-Bonded OH Stretching Modes of Methanol Clusters: A Combined IR and Raman Isotopomer Study. *J. Chem. Phys.* **2007**, *126*, 194307.

(75) Hiatt, R.; Clipsham, J.; Visser, T. The Induced Decomposition of tert-Butyl Hydroperoxide. *Can. J. Chem.* **1964**, *42*, 2754−2757.

(76) Hiatt, R. R.; Mill, T.; Mayo, F. R. Homolytic Decompositions of Hydroperoxides. I. Summary and Implications for Autoxidation. *J. Org. Chem.* **1968**, *33*, 1416−1420.

(77) Oswald, S.; Wallrabe, M.; Suhm, M. A. Cooperativity in Alcohol−Nitrogen Complexes: Understanding Cryomatrices through Slit Jet Expansions. *J. Phys. Chem. A* **2017**, *121*, 3411−3422.

(78) Vogt, E.; Kjaergaard, H. G. Vibrational Spectroscopy of the Water Dimer at Jet-Cooled and Atmospheric Temperatures. *Annu. Rev. Phys. Chem.* **2022**, *73*, 209−231.

(79) Bulychev, V.; Gromova, E.; Tokhadze, K. Experimental and Theoretical Study of the $\nu(HF)$ Absorption Band structure in the H2O...HF Complex. *Opt. Spectrosc.* **2004**, *96*, 774−788.

(80) Vogt, E.; Simkó, I.; Császár, A. G.; Kjaergaard, H. G. Reduced-Dimensional Vibrational Models of the Water Dimer. *J. Chem. Phys.* **2022**, *156*, 164304.

(81) Mackeprang, K.; Kjaergaard, H. G.; Salmi, T.; Hänninen, V.; Halonen, L. The Effect of Large Amplitude Motions on the Transition Frequency Redshift in Hydrogen Bonded Complexes: A Physical Picture. *J. Chem. Phys.* **2014**, *140*, 184309.

(82) Mackeprang, K.; Hänninen, V.; Halonen, L.; Kjaergaard, H. G. The Effect of Large Amplitude Motions on the Vibrational Intensities in Hydrogen Bonded Complexes. *J. Chem. Phys.* **2015**, *142*, 094304.

(83) Mackeprang, K.; Kjaergaard, H. G. Vibrational Transitions in Hydrogen Bonded Bimolecular Complexes - A Local Mode Perturbation Theory Approach to Transition Frequencies and Intensities. *J. Mol. Spectrosc.* **2017**, *334*, 1−9.

(84) Ling, C.; Christian, S. D.; Affsprung, H. E. Vapor Phase Association of Trifluoroacetic Acid with Acetone and Cyclopentanone. *J. Phys. Chem.* **1966**, *70*, 901−904.

(85) Kjaersgaard, A.; Vogt, E.; Christensen, N. F.; Kjaergaard, H. G. Attenuated Deuterium Stabilization of Hydrogen-Bound Complexes at Room Temperature. *J. Phys. Chem. A* **2020**, *124*, 1763−1774.